

Supplementary Information for

“The Nanoscale Structure of the Electrolyte-metal Oxide Interface”

H.-G. Steinrück¹, C. Cao^{1,2}, Y. Tsao³, C. J. Takacs¹, O. Konovalov⁴, J. Vatamanu⁵,

O. Borodin⁵, & M. F. Toney¹

¹SSRL Materials Science Division, SLAC National Accelerator Laboratory, Menlo Park, California 94025, USA

²Department of Materials Science and Engineering, Stanford University, Stanford, California 94305, USA

³Department of Chemistry, Stanford University, Stanford, CA 94305, USA

⁴ESRF, 6 Rue Jules Horowitz, B.P. 220, 38043 Grenoble Cedex, France

⁵Electrochemistry Branch, Sensor and Electron Devices Directorate, U.S. Army Research Laboratory, Adelphi, MD 20783, USA

1. Details of molecular dynamics simulations

The simulation setup consisted of two electrodes and electrolyte inserted between electrodes, as illustrated in Figure S1. The electrode surface was modeled as atomically flat, having the atom distribution like in graphene with its basal plane in contact to electrolyte. During simulations, the atomic charges of the graphene layer next to the electrolyte were allowed to adjust due to changes in the electrostatic environment.^{1,2} Specifically, the total electrostatic energy of the system, consisting of the standard pair-wise electrostatic interactions $\sum_{ij} q_i q_j / r_{ij}$ and the work $W = -\sum_i q_i \phi$ required to generate the electrode charges q_i on the electrode atom “ i ” at an imposed electrostatic potential ϕ , was minimized with respect to the fluctuant charges q_i . These minimization conditions result in a system of linear equations which were numerically solved with a conjugate gradient method. The charge equilibration was performed every 250 fs. Following previous work,^{2,3} the electrode charges were Gaussian distributed with widths of 0.5 Å. These widths of Gaussian charges were shown to accurately reproduce the classical behavior of isolated (i.e. in vacuum) test charges near classical conductors.¹ The long range electrostatics was treated with a smooth particle mesh⁴ Ewald⁵ technique adapted for 2D⁶⁻⁸ geometry. The equations of motions were integrated with a time reversible multistep algorithm⁹ and the temperature was controlled with Nose Hoover¹⁰ chains thermostats. The equations of motion were integrated with RESPA multiple time-step algorithm¹⁰ utilizing the following timesteps: i) 0.5 fs step for bonds and bends, ii) 2.5 fs step for dihedrals and non-bonded interactions within 7.5 Å cut off, and iii) 5 fs step for the long-range non-bonded interactions and reciprocal part of sPME.

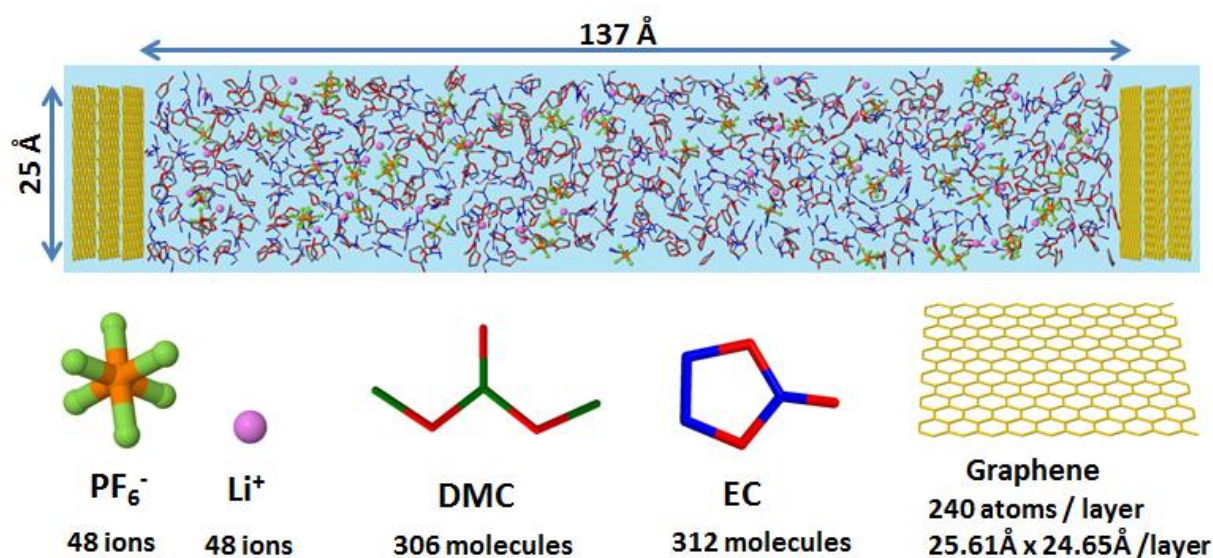


Figure S1: An illustration of the simulation setup, the chemical structures of the electrolyte species, and the electrode surface model. The O atoms in the solvent molecules are represented with red colors, C atoms are shown in green for DMC and blue for EC. To simplify the graphical representation, the H atoms are not shown.

The EC:DMC electrolyte was modeled using a many-body polarizable APPLE&P¹¹ force-field. The functional form of APPLE&P force field is described in ref.⁽¹¹⁾, however, we briefly describe its main features here. It utilizes atomic charges centered on atoms and off-atom positions in conjunction with the atom-centered isotropic dipole polarizability to represent Coulomb and polarization interactions. The induced dipoles are smeared with the Thole screening parameter ($a_T = 0.4$) in order to prevent the so-called “polarization catastrophe” from occurring when non-bonded pairs get closer than $(4\alpha_i\alpha_j)^{1/6}$, where α_i is the polarizability assigned on atom i .^{12,13} The repulsion-dispersion interactions were described using a Buckingham (also called exp-6) potential. The 1-2 and 1-3 force centers were excluded from the charge-charge and repulsion-dispersion interactions. The intramolecular charge-induced dipole interactions were included only between $-\text{CH}_3$ groups from the opposite sides of DMC. No intermolecular charge-induced dipole interactions were included in EC.

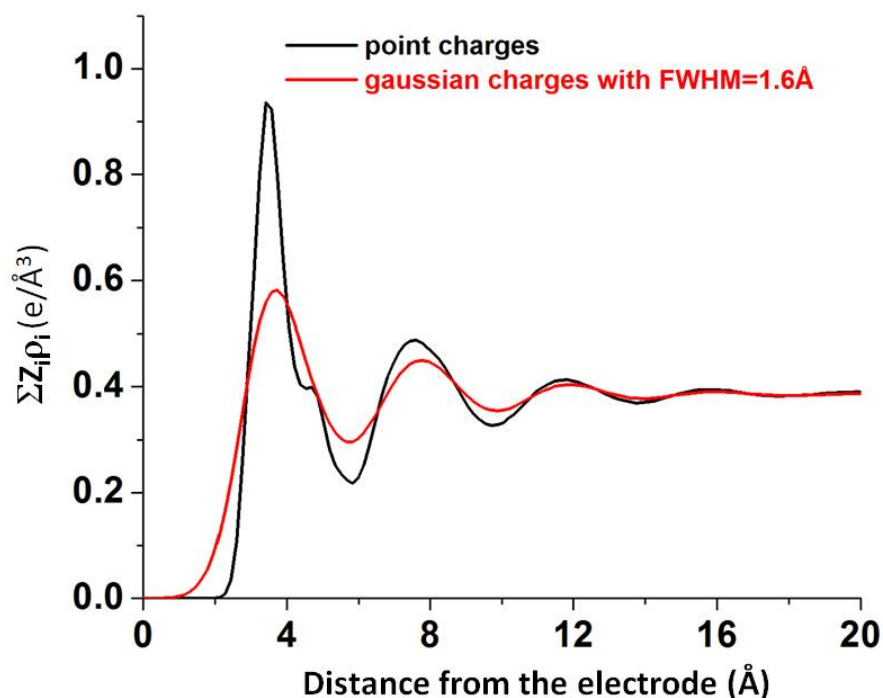


Figure S2.a: The σ profile distribution along the direction perpendicular to the electrode surface, obtained from point charges and Gaussian distributed charges with FWHM = 1.6 Å.

The position of the electrode atoms were constrained during the simulations. The simulation box had a cross section of 25.614 Å x 24.647 Å. Each graphite layer contained 240 atoms. The spacing between layers was 3.35 Å. The graphene layer in direct contact to electrolyte was treated as polarizable, while the other two graphene layers away from electrolyte had their charge set to zero. Their purpose was mainly to improve the description of van der Waals interactions between the electrode and electrolyte, mimicking a

multilayer electrode. The distance between electrodes was adjusted such that the ensemble averaged density in the middle of the simulation box was equal to that calculated for a bulk sample (in 3D periodicity) at atmospheric pressure and the desired temperature.

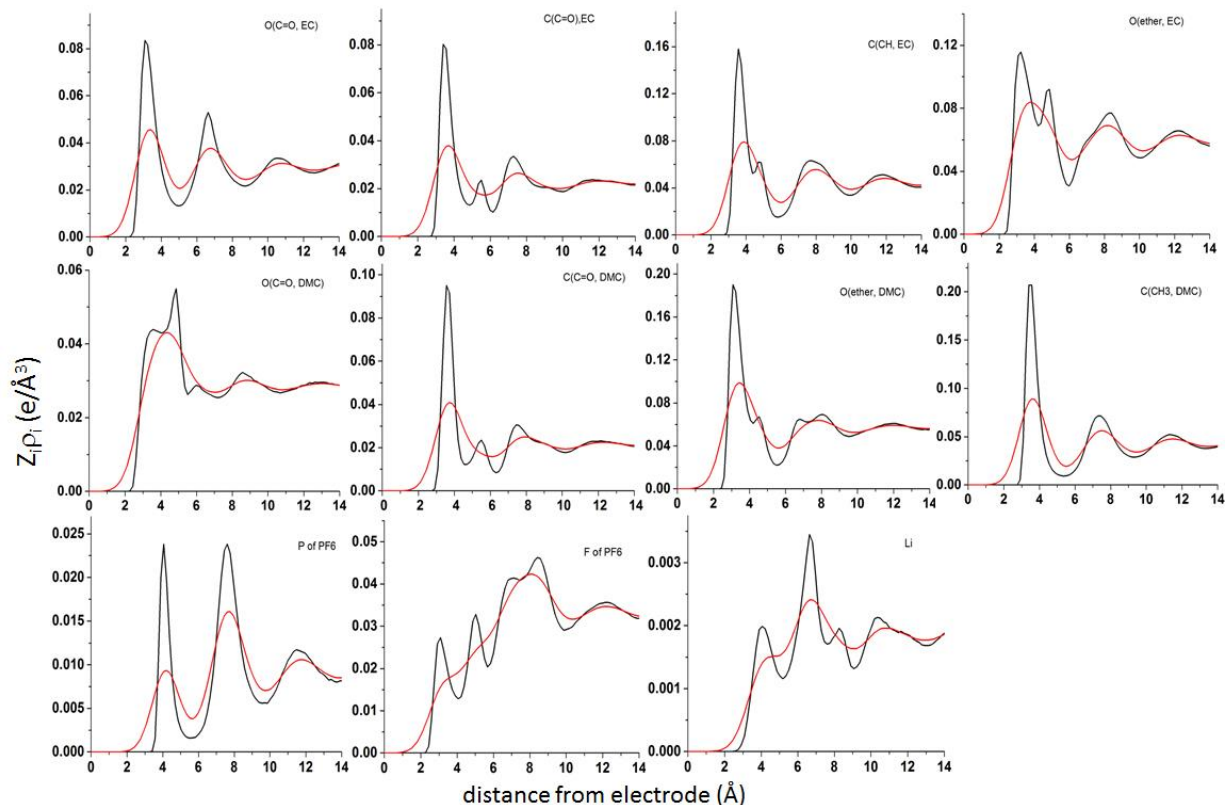


Figure S2.b: The simulated $\rho_i Z_i$ based on point-distributions (black lines) and Gaussian distributions (red lines) as follows, the first row of panels: O(C=O, EC), C(C=O, EC), O(ether, EC), C(CH, EC), the second row of panels: O(C=O, DMC), C(C=O, DMC), O(ether, DMC), C(CH, DMC), and the third row of panels: P (PF6), F(PF6) and Li.

Properties of particular interest for this work were the averaged density profiles of atomic species $\rho_j \equiv \rho_j(z) = \langle \rho_j(x, y, z) \rangle_{x, y}$ and molecular/ionic centers of mass. These density profiles were collected at any 250 fs based on the atoms' distance z from the electrode surface. Additional analysis of the Li^+ cation coordination was done based on configurations saved every 2.5 ps. Reported results are averages of 32 independent trajectories. Total simulation time was ≈ 130 ns for all simulations at 298 K and $\Delta U = 0$ V. In order to calculate electron charge distributions σ from these density profiles, the ρ_j were multiplied with the atomic number Z_j and the obtained profile of $\rho_j Z_j$ was smeared with Gaussian distributions having a FWHM = 1.6 Å. The total estimated electron charge distribution $|\sigma|$ is the sum $|\sigma| = \sum_j \rho_j Z_j$ over all atomic components. The charge distributions σ from point and Gaussian weighed density profiles are shown Figure S2.a. Also, a comparison of the component profiles of $\rho_i Z_i$ based on point versus Gaussian

smearred distributions of ρ_i is shown in Figure S2.b for O and C(solvent) and for P, F and Li(solute). These indicate a layering structure of the electrolyte near the electrode surface, consisting of regions with higher and lower electron density compared to bulk electrolyte. Usage of Gaussian distributions results in a less pronounced structure with the same periodicity as the charge profile obtained from point charges. For component profiles $\rho_i Z_i$ the Gaussian distributions smooth out the local peaks (features) of the density profiles based on point-distributions; see Figure S2.b for groups F, Li, C(C=O, EC and DMC), O(ether, EC), etc.

2. Analysis of the EDL structure for 1M LiPF₆ in EC/DMC 1:1 (weight ratio) obtained from molecular dynamics simulations

Additional insight into the double layer structure was obtained from the analysis of the main contributions from distinct atom types as shown in Figures S3 and S4. These atomic density profiles also show the most pronounced peaks located next to the electrode surface, albeit at different distances and magnitudes suggesting non-random orientation of solvent molecules next to the electrode surface. For example, similar positions of the first peak from EC atoms indicates that EC ring prefers to orient largely parallel to the electrode surface (Figure S3(a-c)), while the carbonyl group (C=O) of DMC slightly prefers to orient away from the surface (Figure S3(d-e)). Solvent structuring modulates ion structure at the interface as evident from the alternating layers the ions Li⁺ and PF₆⁻ (see Figure S3i and Figure 5d in the main manuscript). Such a multilayer structure for the ions is intriguing because it is fundamentally different from the predictions of the basic Gouy Chapman theory.¹⁴⁻¹⁶ As shown in Figure 2 of the main manuscript, similar layering was observed from experiment for more diluted (0.1 M) solutions and from experiment and simulations for the pure solvent. Thus the non-Gouy Chapman behavior observed here for the density profiles of ions does not originates from the surface saturation with ions and ion' exclusion volume (possible when, e.g., the solutions are too concentrated) but instead it is related to the specific intermolecular interactions which lead to a major deviation of the electrolyte solution from the ideal solution considered in the Gouy Chapman model.

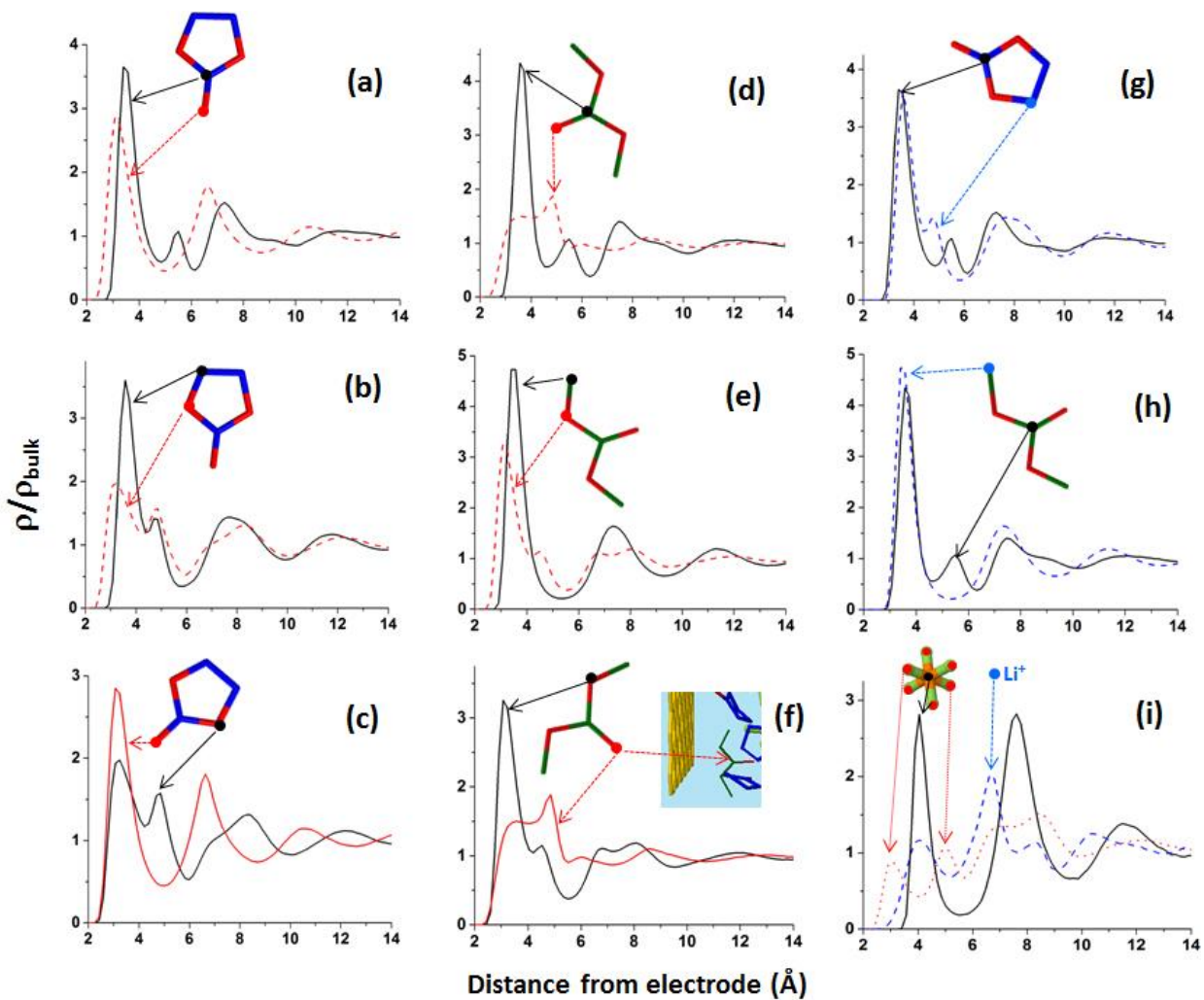


Figure S3: The normalized density profiles $\rho(z)/\rho_{\text{bulk}}$ as a function of the distance z from the electrode surface. Shown are the following groups/atoms: O vs. C atoms involved in carbonyl double bond C=O of (a) EC and (d) DMC, O atoms involved in ether groups vs. C atoms involved in CH(5-ring cycle) or CH₃ for (b) EC and (e) DMC, O atoms involved in carbonyl vs. O ether of (c) EC and (f) DMC, C atoms involved in carbonyl groups vs. C atoms in CH(5-ring cycle) or CH₃ for (g) EC and (h) DMC, and P, F atoms of PF₆ vs. Li ions.

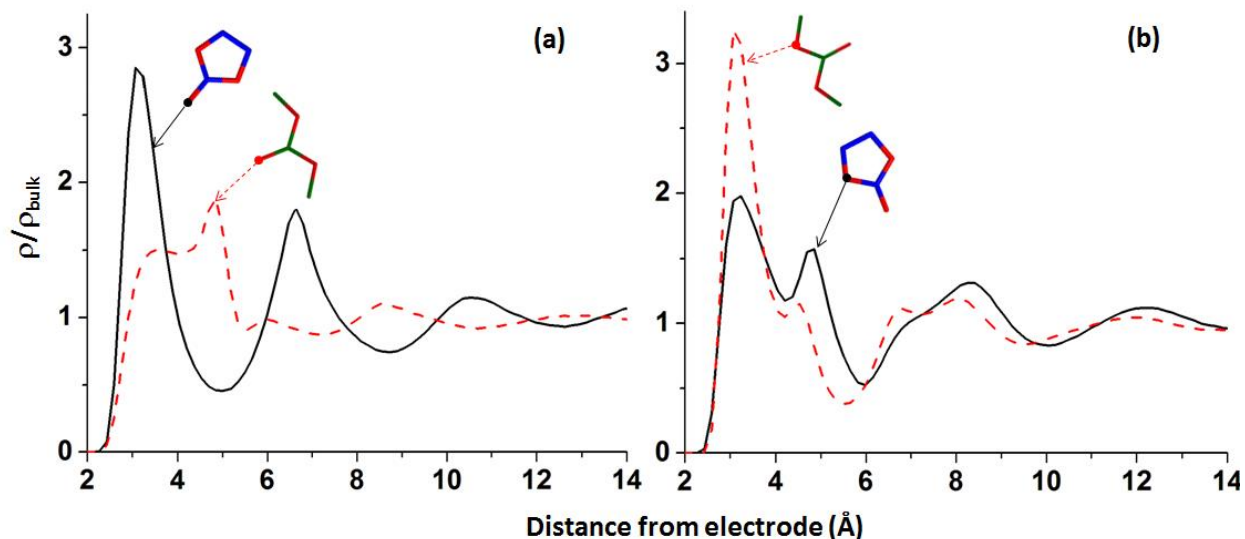


Figure S4: Comparison of the density profiles of the O involved in the double bond C=O (a) and the O involved in the ether bonds (b) for EC vs. DMC. The solid black line represents data for EC and the dashed red line represents data for DM.

The analysis of the distribution of orientations of carbonyl groups relative to the electrode surface shown in Figure S5 confirms the EC tendency to have the C=O vector to orient almost parallel to surface, albeit with a tilt placing the O(C=O, EC) slightly closer to surface than the C(C=O, EC). Such a tilt of the C=O of EC (see Figure S5) is in agreement with the closer location to the surface of the first maximum in density profiles of the O(C=O, EC) than of the C(C=O, EC) shown in S3a, and is consistent with orientations of the EC relative to surface such that both O(ether, EC) and O(C=O, EC) sit on the surface. In contrast to EC, for DMC the C=O (of DMC) vector has an almost random orientation relative to the surface, with only a very slight tendency of O(C=O, DMC) to point away from the surface (see Figure S5). Such an almost random distribution of orientations of C=O of DMC shown in Fig. 6 is in agreement with the much broader density profiles of the O(C=O, DMC) shown in Figure S4a.

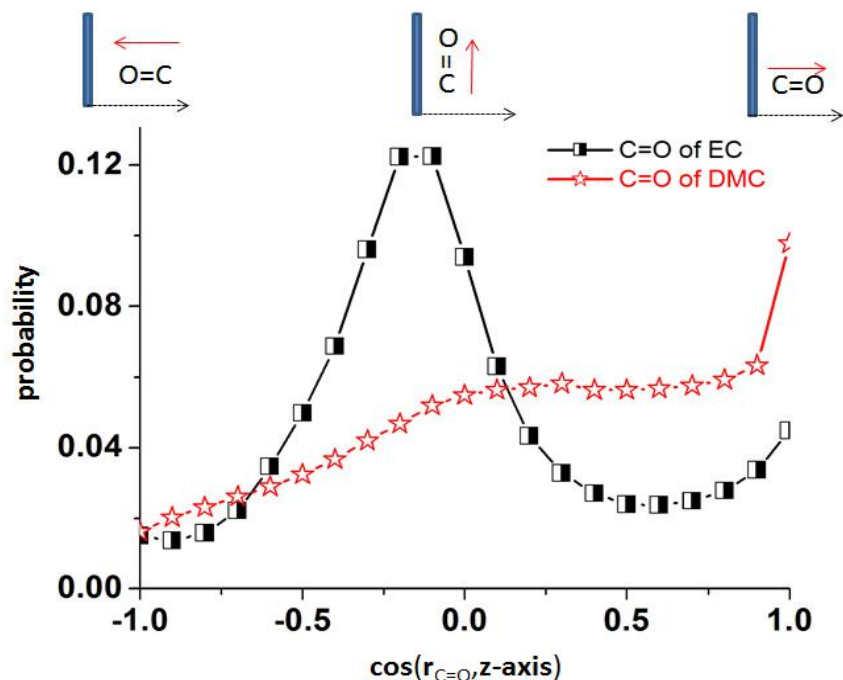


Figure S5: The distribution of the orientations of the vector along the C=O bond relative to our z-axis. The z-axis is defined as the direction perpendicular to the electrode surface. The black line/square symbols represent the C=O of EC and the red line/star symbols represent the C=O of DMC. Note that for a random distribution a constant line will be obtained. A value of zero on the x-axis in the plot corresponds to a perpendicular alignment of the C=O vector with the z-axis and therefore a parallel arrangement of C=O vector with the electrode surface. These distributions are normalized such that the numbers on y-axis sum up to one.

The distribution of orientations of the “elongated axis” of DMC (Figure S5b) confirms a pronounced tendency of DMC to pack parallel to the surface that was concluded from Figure S3-S4. Specifically, it is in agreement with the sharp first peaks in the density profiles of the chemical groups along the DMC’s elongated axis; see e.g. the density profiles of the C(C=O,DMC), O(ether, DMC), and CH₃(DMC) shown in Figures S3d-e, S4b. Such a parallel orientation of the DMC molecule relative to surface does not sterically constrain the O(C=O,DMC) to a specific location resulting in the broader density profile of O(C=O,DMC) in Figure S4a and the almost random distribution of the vector C=O (DMC) relative to surface shown in Figure S5.

Figure S6a shows the orientations of the 5-ring plane of EC relative to the electrode surface plane. About 60% of the interfacial EC is oriented randomly in an angular range $\alpha(5\text{-ring, surface-plane})$ between zero degrees (that corresponds to perpendicular arrangement of 5-ring to surface) to 35 degree tilts between 5-ring and surface. Also, about 30% of the interfacial 5-ring planes are tilted at less than 25 degrees relative to surface plane. In other words, most of EC packs on the surface randomly oriented, however a slight preference towards parallel orientations of the 5-ring plane relative to the surface plane

is observed. This type of distribution of orientations is also apparent in the image snapshot shown in Figure S6a where multiple orientations of EC (relative to the graphene plane) can be observed. Such a distribution of EC orientations (with a certain extent of randomness of 5-ring plane) explains why certain groups have their first maxima of the density profiles slightly closer to surface than other groups, see in Figures S3 a,b,g the closer first maxima in density profiles of O(C=O,EC) than of C(C=O,EC) or of O(ether, EC) than of C(CH,EC). Figure S6b shows the orientations of the “elongated axis” of DMC relative to z-axis. The maximum in the distributions observed an angle of zero between DMC axis and z-axis shows large propensity of DMC sitting parallel on the surface.

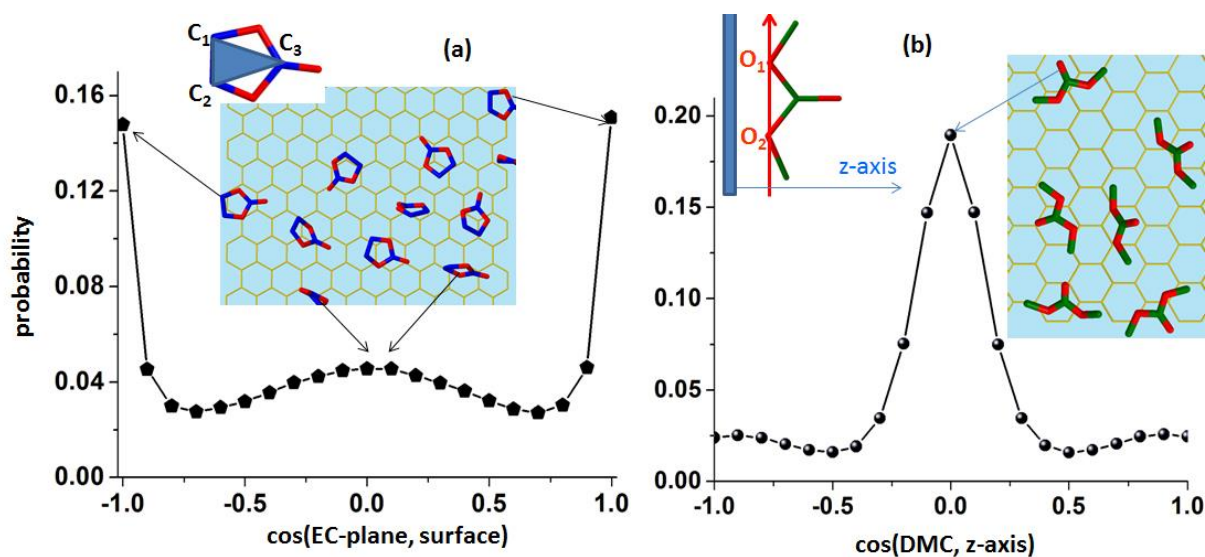


Figure S6: (a) The distribution of the orientations of the 5-ring plane of EC relative to the electrode surface plane. The “5-ring plane” is the plane defined by the three C atoms of EC, as illustrated in the snapshot. (b) The distribution of the orientations of the “elongated direction” of DMC relative to the z-axis. The “elongated direction” of DMC is a vector connecting the two O-ether atoms of DMC, as illustrated in the snapshot. A value of zero in the x-axis of panel (b) corresponds to perpendicularly aligned DMC to z-axis and parallel aligned DMC to the surface. These distributions are normalized such that the numbers on y-axis sum up to one.

Next we examine contributions for the multi-layered electrolyte structure shown in Figure 5 of the main manuscript from individual molecules and atoms. Figure S7 shows the contribution from the point charge distributions $\sigma^{\text{MD-point-distrib}}$ of each solvent molecule and the partial contribution of certain atoms. As shown in Figure S7(a), the O(ether, DMC) and C(CH₃, DMC) groups contribute almost equal to the first peak of σ , however, due to the slight shift (along z-axis) of the location of their first maximum, the resultant peak in σ (summed) signal becomes broadened. The C(C=O, DMC) signal is also sharp, however it is almost half the O(ether, DMC) contribution, as expected from the stoichiometric ratio C(C=O):O(ether) = 1:2 within the molecule. Thus, the contribution of DMC molecule to the first peak of σ reflects the parallel alignment of DMC to surface and it can be accounted from the chemical groups

along the “elongated axes” of the adsorbed DMC (see Figures S7(a,c)). Surprisingly, the O(C=O, DMC) has little contribution to the first peak of σ and it rather broadens it.

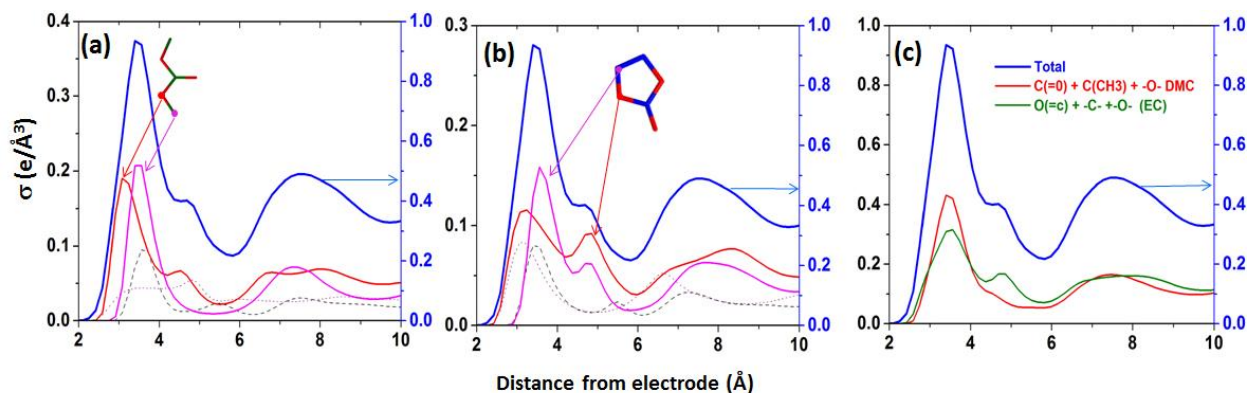


Figure S7: The simulated signal $\sigma = \sum \rho_i z_i$ based on point-distributions for individual molecules (a) DMC and (b) EC and for the total (summed) σ (c). The dashed line in panels (a) and (b) are for C(C=O) and the dotted lines in panels (a) and (b) are the contributions from O(C=O). A double y axis is utilized and the values of the solid blue lines are represented in the right-side y-axis (blue) while the other profiles are represented by left y axis.

For the EC molecules, the C(CH, 5-ring) together with the C and O atoms involved in C=O sharpens the first peak of σ while the O(ether) broadens it to some extent (Figure S7(b)). The molecules EC and DMC contribute almost equally to the first peak of σ , however, due to more random orientations of 5-ring EC, the contribution $\sum Z_i \rho_i$ from EC molecule to total σ is broader than the corresponding contributions from DMC which adsorbs to a large extent parallel to surface (Figure S8(c)).

Next, we analyzed the structure of the Li^+ first solvation shell at the interfacial layer. As observed for bulk electrolyte, the Li^+ cations are coordinated primarily by carbonyl groups of EC with a smaller contribution from DMC. The relative populations of EC and DMC in the Li^+ solvation shell are similar for bulk and interfacial electrolyte, i. e. within a 6 Å from electrode surface. Specifically, the coordination number of the Li^+ cation with EC is 2 in near surface and 2.1 in bulk and the coordination number of Li with DMC is 1.6 in bulk and 1.3 near surface. This indicates that as a Li^+ approaches the surfaces and starts desolvation it prefers to desolvate DMC first in agreement with our previous findings.^{17,18}

We also examined the influence of salt on the interfacial solvent structure by comparing density profiles ρ/ρ_{bulk} of O(carbonyl) from EC and DMC as shown in Figure S9. Addition of salt slightly increases the first peak in the DME profile (Fig. S9a), while slightly decreasing the first peak in the EC profile (Fig. S9b). The cumulative profile of the EC and DMC carbonyl oxygen atoms shown in Fig. S9c is essentially unchanged, with a small increase of the relative peak height of the DMC’s peak corresponding to molecules with their carbonyl group further separated from the surface (indicated by the

blue arrow). This is consistent with the XRR-derived suggestion of a slight reorientation of the molecules in the presence of ions, which results an increased measured d -spacing.

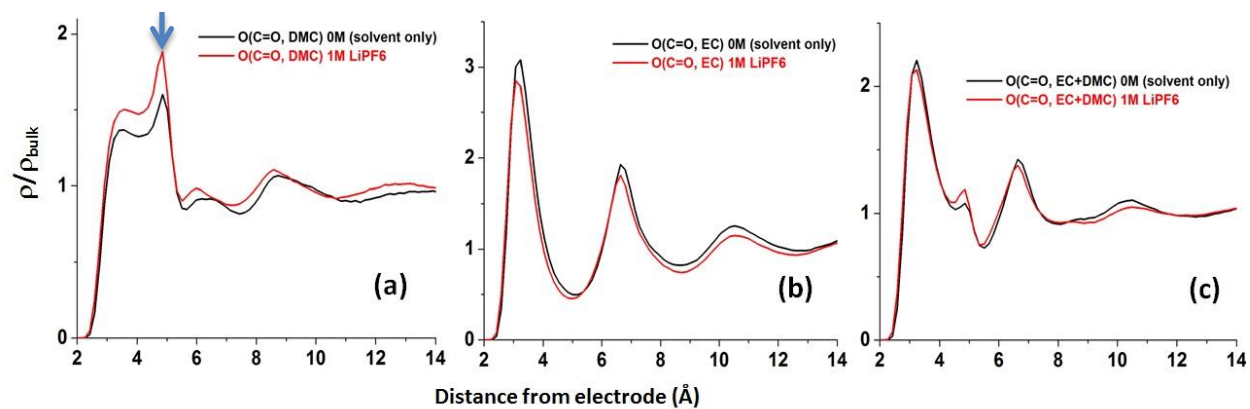


Figure S9. A comparison of the density profiles of O(C=O) 0M vs 1V for (a) DMC, (b) EC, and (c) the summed contribution for both EC and DMC.

References:

- 1 J. I. Siepmann and M. Sprik, *J. Chem. Phys.*, 1995, **102**, 511–524.
- 2 S. K. Reed, O. J. Lanning and P. A. Madden, *J. Chem. Phys.*, , DOI:10.1063/1.2464084.
- 3 J. Vatamanu, O. Borodin and G. D. Smith, *Phys. Chem. Chem. Phys.*, 2010, **12**, 170–182.
- 4 U. Essmann, L. Perera, M. L. Berkowitz, T. Darden, H. Lee and L. G. Pedersen, *J. Chem. Phys.*, 1995, **103**, 8577–8593.
- 5 P. P. Ewald, *Ann. Phys.*, 1921, **64**, 253.
- 6 M. Kawata and U. Nagashima, *Chem. Phys. Lett.*, 2001, **340**, 165–172.
- 7 M. Kawata and M. Mikami, *Chem. Phys. Lett.*, 2001, **340**, 157–164.
- 8 M. Kawata, M. Mikami and U. Nagashima, *J. Chem. Phys.*, 2002, **116**, 3430–3448.
- 9 G. J. Martyna, M. E. Tuckerman, D. J. Tobias and M. L. Klein, *Mol. Phys.*, 1996, **87**, 1117–1157.
- 10 W. G. Hoover, *Phys. Rev. A*, 1985, **31**, 1695–1697.
- 11 O. Borodin, *J. Phys. Chem. B*, 2009, **113**, 11463–11478.
- 12 D. Elking, T. O. M. Darden and R. J. Woods, *J. Comput. Chem.*, 2007, **28**, 1261–1274.
- 13 B. T. Thole, *Chem. Phys.*, 1981, **59**, 341–350.
- 14 G. Gouy, *Comptes Rendus Hebd. Des Seances L Acad. Des Sci.*, 1909, **149**, 654–657.
- 15 K. B. Oldham, *J. Electroanal. Chem.*, 2008, **613**, 131–138.
- 16 A. A. Kornyshev, *J. Phys. Chem. B*, 2007, **111**, 5545–5557.
- 17 J. Vatamanu, O. Borodin and G. D. Smith, *J. Phys. Chem. C*, 2011, **116**, 1114–1121.
- 18 O. Borodin and D. Bedrov, *J. Phys. Chem. C*, 2014, **118**, 18362–18371.